Journal for ImmunoTherapy of Cancer

Tissue-resident memory T cells from a metastatic vaginal melanoma patient are tumor-responsive T cells and increase after anti-PD-1 treatment

Angela Pizzolla ,[1,2] Simon Paul Keam ,[1,3,4] Ismael A Vergara,[3,5,6] Franco Caramia,[1,4] Niko Thio,[3] Minyu Wang ,[1,2] Nikolce Kocovski,[2] Daniela Tantalo,[2] Jafar Jabbari,[7] George Au-Yeung,[8,9] Shahneen Sandhu,[1,9] David E Gyorki,[10] Alison Weppler,[9] Maurizio Perdicchio,[11] Grant A McArthur,[3,8] Anthony T Papenfuss,[1] Paul Joseph Neeson [1,2]

To cite: Pizzolla A, Keam SP, Vergara IA, *et al*. Tissue-resident memory T cells from a metastatic vaginal melanoma patient are tumor-responsive T cells and increase after anti-PD-1 treatment. *Journal for ImmunoTherapy of Cancer* 2022;**10**:e004574. doi:10.1136/jitc-2022-004574

► Additional supplemental material is published online only. To view, please visit the journal online (http://dx.doi.org/10.1136/jitc-2022-004574).

AP and SPK contributed equally.

Accepted 05 April 2022

For numbered affiliations see end of article.

Correspondence to
Dr Angela Pizzolla;
angela.pizzolla@petermac.org

Dr Paul Joseph Neeson;
paul.neeson@petermac.org

ABSTRACT

Background Vaginal melanoma (VM) is a rare cancer and has a poor response to immune checkpoint blockade (ICB). $CD8^+$Tissue Resident Memory (TRM) T cells proliferate in response to ICB and correlate with longer survival in metastatic cutaneous melanoma. However, their capacity to respond to VM and their neoantigens is not known.

Methods Using longitudinal samples, we explored the evolution of VM mutations by whole-exome sequencing and RNAseq, we also defined the immune context using multiplex immunohistochemistry and nanostring pan cancer immune profile. Then using fresh single cell suspensions of the metastatic samples, we explored VM T cells via mass cytometry and single cell RNAseq and T cell receptor sequencing (TCRseq). Finally, we investigated TRM, pre-TRM and exhausted T cell function against melanoma neo-antigens and melanoma differentiation antigens in vitro.

Results Primary VM was non-inflamed and devoid of $CD8^+$ TRM cells. In contrast, both metastases showed proliferating $CD8^+$ TRM were clustered at the tumor margin, with increased numbers in the second ICB-refractory metastasis. The first metastasis showed dense infiltration of $CD8^+$ T cells, the second showed immune exclusion with loss of melanoma cell Major histocompatibility complex (MHC)-I expression associated with downregulation of antigen presentation pathway gene expression. $CD8^+$ TRM from both metastases responded to autologous melanoma cells more robustly than all other $CD8^+$ T cell subsets. In addition, $CD8^+$ TRM shared TCR clones across metastases, suggesting a response to common antigens, which was supported by recognition of the same neoantigen by expanded tumor infiltrating lymphocytes.

Conclusions In this study, we identified TRM clusters in VM metastases from a patient, but not primary disease. We showed TRM location at the tumor margin, and their superior functional response to autologous tumor cells, predicted neoantigens and melanoma differentiation antigens. These $CD8^+$ TRM exhibited the highest tumor-responsive potential and shared their TCR with tumor-infiltrating effector memory T cells. This suggests VM metastases from this patient retain strong antitumor T cell functional responses; however, this response is suppressed in vivo. The loss of VG MHC-I expression is a common immune escape mechanism which was not addressed by anti-PD-1 monotherapy; rather an additional targeted approach to upregulate MHC-I expression is required.

Key messages

⇒ Tissue resident memory T cells (TRM) are prognostic of improved survival in melanoma and proliferate during immune checkpoint inhibitor therapy. The role of TRM in melanoma and in the rare subtype of vaginal melanoma is unknown. In a case study of metastatic vaginal melanoma, we sampled separate sites before and after immunotherapy and we show that TRM are increased after immunotherapy. Moreover, TRM from metastatic sites both before and after immunotherapy respond to tumor cells in vitro, and do so more robustly than other T cell subsets. Decreased Major histocompatibility complex (MHC)-I expression on tumor cells after immunotherapy might be a reason of TRM inability to clear the tumor in vivo. This study demonstrates that TRM can recognize vaginal melanoma tumor cells ex vivo and suggests that interventions that can increase MHC-I expression in tumor cells might be a key player in reactivating the immune system in melanoma.

INTRODUCTION

Primary melanoma of the female genital tract is a rare disease, comprizing 1% of all melanomas,[1] female genital tract melanoma originate more commonly in the vulva (80%) than the vagina (20%).[1 2] The 5-year survival rate for vaginal melanoma (VM) is poor (27%).[3] Reasons for this poor clinical outcome are not completely understood but do include

frequent (40%) clinical presentation with regional or distant metastasis and drug resistant disease.[3] In addition, nearly 80% of VM primary disease will recur post-surgery.[4] VM has distinct molecular features including *BRAF* mutations (26%), and higher rates of *KIT* mutation (27%) than that observed in cutaneous melanoma (8.8%).[5 6] In clinical trials with immune checkpoint blockade (ICB), VM patients were included in a mucosal melanoma cohort including patients with head and neck, anal and urogenital disease. Clinical response rates to single or dual ICB were reduced in mucosal versus cutaneous melanoma although the safety profile was similar,[7] possibly because mucosal melanomas are less immunogenic due to a decreased tumor mutation burden.[8]

Mucosal and cutaneous melanoma with tumor-infiltrating lymphocytes (TILs) are associated with a lower risk of distant metastasis.[9 10] However, only 30% of primary oral mucosal melanoma samples contained TILs[10] and due to the rarity of the disease, there is limited understanding of the immune context of mucosal melanoma arising at other sites, including VM. Recently, $CD8^+$ T cells and in particular tissue-resident memory $CD8^+$ T cells ($CD8^+$ TRM) were prognostic for overall and disease-free survival in metastatic cutaneous melanoma.[11 12] Furthermore, $CD8^+$ TRM proliferate in response to pembrolizumab treatment.[11] In animal models, $CD8^+$ TRM have a pivotal role in melanoma immunosurveillance.[13 14] However, the $CD8^+$ TRM profile in VM has not been yet explored. To interrogate this question, we employed a unique set of longitudinal tumor samples of primary and metastatic VM from a immunotherapy resistant patient. The metastases were collected before and after ICB, were clonally related, and maintained a low mutational burden and shared a similar neoantigen profile. We investigated the immune context in primary and metastatic disease with a focus on $CD8^+$ TRM cells and we explored T cell functionality, phenotype and T cell receptor (TCR) repertoire sharing.

MATERIALS AND METHODS

Patient samples

The patient was diagnosed with stage 3 metastatic melanoma and underwent clinically indicated surgery after being enrolled in a prospective study approved by the Peter MacCallum Cancer Centre (PeterMac) human ethics research committee (13/141). We received representative fragments of fresh sterile tissue after surgery, from which we: (1) froze tumor pieces, (2) cultured others in high dose IL-2 for 2–4 weeks till we obtained 1×10^8 of in vitro expanded TILs,[15] (3) mechanically and enzymatically digest the remaining tissue to obtain a single cell suspension which was then frozen, as previously described.[16] We also accessed formalin-fixed paraffin-embedded (FFPE) tissues through pathology.

Multiplex immunohistochemistry (mIHC) was performed as described previously[16] with modifications detailed in online supplemental material.

Mass cytometry

Frozen cells were thawed in warm 30 mL of RPMI with 20% heat-inactivated fetal calf serum and 30 U/mL of DNAse I (Roche) and manually counted excluding Trypan Blue (Sigma) positive cells. Staining protocol and the full list of antibodies used is in online supplemental methods and table 3. All CyTOF samples were preprocessed through Cytobank which includes bead standard normalization, spill-over correction, and pregated for singlet, live cells and CD45 and HLA-ABC expression to identify TILs. Each sample expression matrix is transformed using arcsinh with cofactor 5. Clustering is performed on pooled samples, using FlowSOM method,[17] which was run through CATALYST R package.[18] Metaclustering of FlowSOM clusters was performed using ConsensusClusterPlus[19] algorithm, which is also available in CATALYST package. Markers included for clustering are included in online supplemental methods. UMAP calculation for two-dimensional visualization was performed through R package uwot.[20] Heatmaps were generated using R package ComplexHeatmap,[21] violin and scatter plots were generated using R package ggplot2.[22]

Single cell RNA sequencing

Cells were thawed as described above and manually counted. 1e6 cells per samples were stained with viability dye (LIVE/DEAD Fixable Near-IR Dead cell stain, Invitrogen). Fc receptors were blocked by staining with Human BD Fc Block (BD) in FACS buffer (PBS (Ca^{++}/Mg^{++} free), 2% FBS, 2 mM EDTA). Cells were stained with 50 µ L of antibody cocktail containing anti-CD3 BV711, anti-CD45 BV510, anti-CD19 APC-cy7 and anti-CD11c APC-Fire 750 as a dump channel. Cells were sorted as live $CD3^+$ $CD45^+$ $CD11c^-$ $CD19^-$ lymphocytes on BD FACSAria Fusion five equipped with a 100 µm nozzle (BD Biosciences). Cells were manually counted and concentration adjusted to 1 or 2×10^6 cells/mL in PBS or PBS containing (400 µg/mL) BSA and 0.2 U/µL of Protector RNase Inhibitor (Roche). About 20,000 cells were loaded onto the Chromium Controller (10X Genomics) according to manufacturer's instructions and single cell RNA and VDJ libraries were constructed using the Single Cell Immune Profiling solution kit (10X Genomics). 5' gene expression and VDJ libraries were sequenced on Illumina HiSeq (2×100 cycles) and Illumina NextSeq Mid Output (2×150 cycles) platforms, respectively, at Australian Genome Research Facility. Raw FASTQ read data from high throughput sequencing, including gene expression data and TCR sequencing of 10x libraries were processed using conventional *cellranger* (10x Genomics) pipelines. Subsequent QC data analysis including TCR repertoire and cell phenotype clustering and visualization was performed using script integration[23] and Seurat V.3.0 (23), respectively.

Twenty-four-hour T cell activation assay

Thawed live cells were stained with and anti-CD103 BV421, anti-CD45 BV510, anti-CD8 BV605, anti-CCR7 BV711, Anti-CD45Ro BV785, anti-CD69 PEcy7, anti-CD4

AF700 and anti-CD19 APC-cy7, anti-CD11c APC/Fire 750 (all from Biolegend), prior to sorting as above. Live melanoma cells (CD45$^-$ SSC-A^{high} FSC-A^{high} cells) and three populations of CD8$^+$ CD4$^-$ T cells were sorted, the latter as live CD11c$^-$ CD19$^-$ CD45$^+$ CD45Ro$^+$ CCR7$^-$ lymphocytes distinguished by the marker combination CD69$^+$ CD103$^-$, CD69$^+$ CD103$^+$ and CD69$^-$ CD103$^-$.

T cells were stained with anti-PD1(pembrolizumab) or Isotype IgG$_4$ (BD). T cells and melanoma cells were cultured for 24 hours at a 2:1 effector to target ratio with anti-CD107a-AF488 antibody (Biolegend) or BD GolgiPlug (Brefeldin A) in complete human media (online supplemental methods). For non-sorted samples, 50,000 cells from tumor samples or 25,000 cells from expanded TILs were cocultured.

After 24 hours, cells were restained with all the extracellular markers used for sorting, adding anti-41BB-PercP-Cy5.5 (Biolegend) to anti-CD107a stained cells. Cells incubated with GolgiPlug were permeabilized with eBioscience FoxP3/Transcription Factor Staining Buffer Set (Invitrogen) prior to intracellular staining with anti-IFNγ-PEDazzle594, anti-TNFα-APC, anti-Granzyme B-FITC and IL-2-PercPCy5.5 (all Biolegend).

10 day T cell-tumor cocultures

T cells were sorted from Met1 and Met2 tumor digest as described above.

Met1 and Met2 tumor cells lines were derived from sorted tumor cells and cultured in RPMI 1640 (Gibco) supplemented with 10% FCS, 100 U/mL Penicillin, 100 µg/mL Streptomycin and 2 mM L-Glutamine (RPMI-10%) and were stimulated with 2 ng/mL of recombinant human IFNγ (Biolegend) for 3 days before coculture with sorted T cells.

T cells were cultured at 1:1 ratio with tumor cell line irradiated with 30 cGy in complete human media, in presence of rhIL7 and IL15 (both Peprotech, 25 ng/mL) and human IL-2 (Peprotech, 20 U/mL), the last one added only from day 3 of culture. Half of the media was changed every second day. On day 11, one-third of the cells were restimulated with one-third of the original numbers of tumor cells in the presence or absence of BD GolgiPlug (Brefeldin A). Cells were stained as described above adding anti-CD25 BV605 (Biolegend).

T cell function responses to predicted neoantigens

Lymphoblastic cell lines (LCLs) were generated from patient's PBMC by infecting them with Epstein Barr Virus in presence of ciclosporin A. Tumor cells were stimulated with 2 ng/mL of recombinant human IFNγ (Biolegend) for 3 days before coculture with expanded TILs.

LCL and IFNγ stimulated-tumor cell lines expressed Major histocompatibility complex (MHC) I and II as detected by flow cytometry (data not shown) and were irradiated at 30 Gy before coculture with T cells. LCLs were loaded with peptide pools and cocultured with expanded TILs at 1:1 ratio in complete human media, additioned with human IL-2 (100 U/mL), rhIL7 and IL15 (25 ng/mL). Half of the media was replaced on day 4 and on day 7 the cells were resuspended in complete human media containing only IL2 (20 U/mL), until day 11. As controls, cells were stimulated with Immunocult aCD3/CD28 (StemCells), 5 µL per 200 µL of media or with culture media alone. On day 11, one-fourth of cultured T cells were added to either irradiated LCL pulsed with peptide pools, or to autologous tumor or Immunocult, maintaining the same stimulation as during the 11 days, in the presence of anti-CD107a-Alexa Fluor 488 or BD Golgi Plug. As control, cells are stimulated with PMA. After 3.5 hours at 37°C, cells were stained as described in the 24 hr T cell activation assay. Peptides were purchased from GenScript, pooled according to the protein of origin and indicated in online supplemental tables 4–6.

Details for genomics analysis including whole exome sequencing, RNAseq, nanostring immune gene expression profile, and the bioinformatic analysis associated with neo-antigen prediction are also in online supplemental material.

RESULTS

TRM cells cluster on the tumor margin and are enriched after immunotherapy

We collected fresh and FFPE tissue samples from two subcutaneous metastases of a patient with VM. After diagnosis in 2010, the tumor developed resistance to multiple lines of treatments, including radiation, chemotherapy and immunotherapy comprizing four doses of ipilimumab in 2012 and pembrolizumab from 2014 (online supplemental figure S1 and clinical history in the legend). The first metastasis (Met1) was excised from the central back in 2014, 2 years after ipilimumab and prior to receiving pembrolizumab. The second metastasis (Met2) is a metastasis in the right shoulder (occurring in 2015) and resected after 1 year of mixed response to pembrolizumab. To investigate the immune landscape, we performed mIHC on the primary and metastatic melanoma FFPE samples (figure 1A–C). The primary sample was almost devoid of immune cells, except for a small island of CD4$^+$ T cells and CD4$^+$ FoxP3$^+$ Tregs, characterizing it as a non-inflamed tumor. In contrast, Met1 was an inflamed tumor and had a dense infiltration of CD8$^+$ T cells (figure 1A–D). Met2 presented a third profile, characterized by immune exclusion (figure 1A and D–E). CD8$^+$CD103$^+$ TRM cells were absent in the primary disease, present only in a small area near the margin of Met1 and increased in number in Met2, mainly at the tumor margin (figure 1A,D). Direct cell to cell interaction occurs within a 10–20 µm radius. In the primary sample, all T cell types were at a similar median distance to the tumor of about 40 µm, suggesting minimal direct interaction with tumor (figure 1E). In contrast, in Met1 CD4$^+$ T cells, Tregs and CD8$^+$ T cells were directly interacting with the tumor, with a median distance of 20 µm, while CD8$^+$CD103$^+$ TRM were more distant (figure 1E).

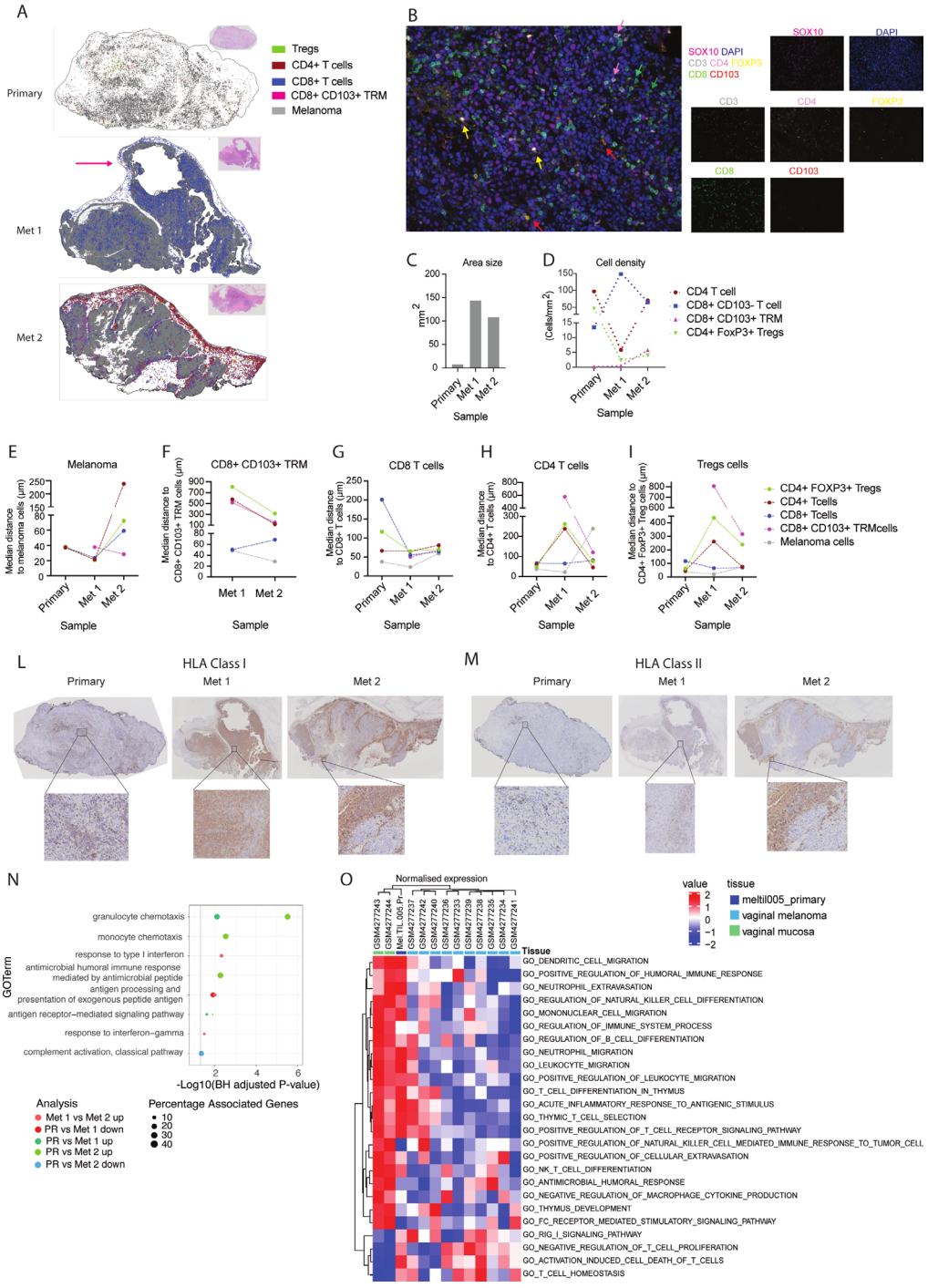

Figure 1 CD8$^+$ TRM cells clustered at the tumor margin and were more proximal to vaginal melanoma cells than other T cells (A) H&E staining and multiplex IHC spatial plots of the three tumor samples where each dot represents a cell: melanoma (SOX10$^+$ DAPI$^+$), CD4$^+$ T cells (DAPI$^+$ CD3$^+$ CD4$^+$), CD4$^+$ Tregs (DAPI$^+$ CD3$^+$ CD4$^+$ Foxp3$^+$), CD8$^+$ T cells (DAPI$^+$ CD3$^+$ CD8$^+$CD103$^-$), CD8$^+$ CD103$^+$ TRM (DAPI$^+$ CD3$^+$ CD8$^+$CD103$^+$). Magenta arrow: are with CD8$^+$ CD103$^+$ TRM. (B) Representative image of fluorescent staining, depicting the black boxed area in the metastatic sample. Red arrow: CD3$^+$ CD8$^+$ CD103$^+$ T cell, yellow arrow: CD3$^+$ CD4$^+$ Foxp3$^+$ Tregs, pink arrow: CD3$^+$ CD4$^+$ T cells, green arrow: CD3$^+$ CD8$^+$ T cells. (C) Area (mm^2) of each tumor sample. (D) Density of each cell type in the melanoma samples. (E–I) Spatial relationship (um)between TRM cells and melanoma, and TRM with other T cell subsets. (L, M) MHC-I and MHC-II expression detected by IHC staining of FFPE tissue. (N) Bubble plot of differentially expressed pathways between the three specimens as identified by ClueGO in Cytoscape on differentially expressed called genes by nSolver. P value is adjusted with Benjamini-Hochberg correction. In shades of red, the pathways upregulated in Met 1, in shades of green the ones in the primary and in turquoise the one in Met2. (O) Heatmap of significantly ($p<0.05$) differentially expressed pathways between normal vaginal mucosa and vaginal mucosal melanoma from,[3] determined by GSVA on the 137 genes overlapping between the nCounter Nanostring PanCancer Immune Profiling and the PanCancer 360 IO. The heatmap was then calculated including the primary samples from our study too. FFPE, formalin-fixed paraffin-embedded; GSVA, Gene Set Variation Analysis; IHC, immunohistochemistry; TRM, tissue resident memory.

In Met2, TRM cells interacted closely with melanoma and CD8+ T cells but were spatially more distant to other cell types (figure 1F). Taken together, while CD8+ T cell infiltration was heterogeneous between metastases, the TRM cells clustered at the tumor margin adjacent to tumor cells.

The tumor immune context evolved during disease progression

MHC-I and II expression on tumor cells was heterogenous in all samples, with a mark reduction of both in Met2, particularly in tumor nests that were immune excluded (figure 1L,M). Targeted gene expression performed with Nanostring nCounter CancerPanImmune panel and 30 custom added genes (online supplemental table 1) confirmed this observation, with significantly higher antigen presentation pathways expressed in Met1 compared with the primary and Met2 (figure 1N and online supplemental table 2). Consequently, Met1 expressed significantly higher type I interferon (IFN) and IFN-γ response pathways compared with Met2. This could which could be due to higher T cell infiltration, response to chemotherapy and/or radiotherapy (RT) and a mechanism to tumor evasion from both treatments[24] (figure 1N). Both metastases show higher upregulation of T cell genes, immune checkpoint, cytotoxic factors, chemokines known to attract T cells and higher tumor inflammatory signature genes compared with the primary sample (online supplemental figures S2A,B), reflecting the higher infiltration of CD4+ and CD8+ T cells observed by mIHC (figure 1A–C). Compared with the metastatic samples, the primary disease showed increased antigen receptor-mediated signaling pathways, mediated by FoxP3 (figure 1N and online supplemental table 2), which matched the increased Treg infiltration observed by mIHC (figure 1D), as well as granulocytes and monocytes recruitment, which included the antimicrobial humoral response pathway (figure 1N and online supplemental table 2).

Met2 displayed higher complement pathway compared with the primary, which was corroborated by identification of higher B cell function in both metastases compared with the primary via whole genome RNA sequencing analysis (online supplemental figure S2C). mIHC staining indeed showed B cell aggregates resembling tertiary lymphoid structures at the margin of Met2 and broad B cell infiltration in Met 1 (online supplemental figure S2D,E).

To understand how the primary disease sample related to other VM, we compared the gene expression of the primary disease with the only publicly available dataset of vaginal mucosal melanoma and of healthy vaginal mucosa.[25] Using principal component analysis, the primary disease sample immune gene expression profile is distinct from healthy vaginal mucosa (online supplemental figure S2F), and also has overlap with other mucosal melanoma subtypes (online supplemental figure S2G). GSVA pathway analysis showed the primary disease sample had higher immune cell infiltration compared with the published VM cohort but similar negative regulation of T cells (figure 1O). This analysis confirmed that primary VM are immunologically cold, while metastases can display an immune excluded or hot phenotype.

Metastatic VM is infiltrated by TRM cells with high immune checkpoint expression

We characterized the phenotype of TILs in Met1 and Met2, as well as expanded TILs from both samples (Met1 exp and Met2 exp), using a 40-parameter mass cytometry panel (online supplemental table 3 and online supplemental figure S3). Non-immune cells (including tumor cells) were identified as CD45- and expressed HLA-ABC (93% vs 85%), HLA-DR (63% vs 45%) and PDL1 (13% vs 8%) in Met1 and Met2 (figure 2A). Live TILs (SOX10- CD45+ HLA-ABC+ cells) from the tumor and expanded TILs clustered separately indicating major differences in their marker expression, except for specific CD8+ and CD4+ T cell clusters that were shared across the samples (figure 2B–D). Compared with T cells in expanded TILs, CD8+ (and to a certain extent also CD4+) T cells in tumor samples were characterized by higher expression of immune checkpoint molecules (PD1, CTLA4) and lower expression of TCF1, FABP5, CXCR6 and activation and proliferation markers (HLA-DR, Ki67), indicating that expansion condition favors self-renewal and activation (figure 2F and online supplemental figure S3C).

CD8+ T cells in tumor samples were effector memory (CD45RA- CD62L-) and comprised three clusters: CD8+CD103+ TRM, CD8+CD69+CTLA4+ T cells and CD8+CD69intCD39- T cells (figure 2D–E). TRM cells percentage increased from Met1 to Met2 (figure 2D). CD8+ TRM and CD8+CD69+CTLA4+ T cells were phenotypically very similar and differed only by higher CD103 and CXCR6 expression on TRM cells (figure 2F–H). Compared with CD8+CD69int CD39- T cells, CD8+CD103+ TRM and CD8+CD69+CTLA4+ T cells expressed higher levels of CD39, a marker of tumor-specific T cells,[26] higher immune checkpoint molecules (PD1, TIGIT, TIM3 and CTLA4) and higher levels of the exhaustion marker TOX and tissue retention markers (CD69, CXCR6, CD103), indicating that CD8+CD103+ TRM and CD8+CD69+CTLA4+ T cells are tissue-resident and partially exhausted or dysfunctional T cells. CD8+CD69int CD39- T cells may be circulating cells with a higher self-renewal capacity (TCF1intermediate) (figure 2F–I). The only difference between CD8+ and CD4+ T cells in Met1 and Met2 was the lower PD1 expression in Met2 compared with Met1 (figure 2G–I, online supplemental figure S3). This is due to competitive binding of pembrolizumab to PD-1 on T cells in Met2 (figure 3). Macrophages and dendritic cells were present in TILs in both metastatic samples and had a very similar phenotype, with high expression of HLA-DR, FABP5, CD39 and PDL1 (figure 2F and online supplemental figure S3B). B cells were not detected in either metastatic sample. Overall, in vitro expansion favored the expansion of highly proliferating CD8+ T cells and cytotoxic cells. The T cell clusters were similar

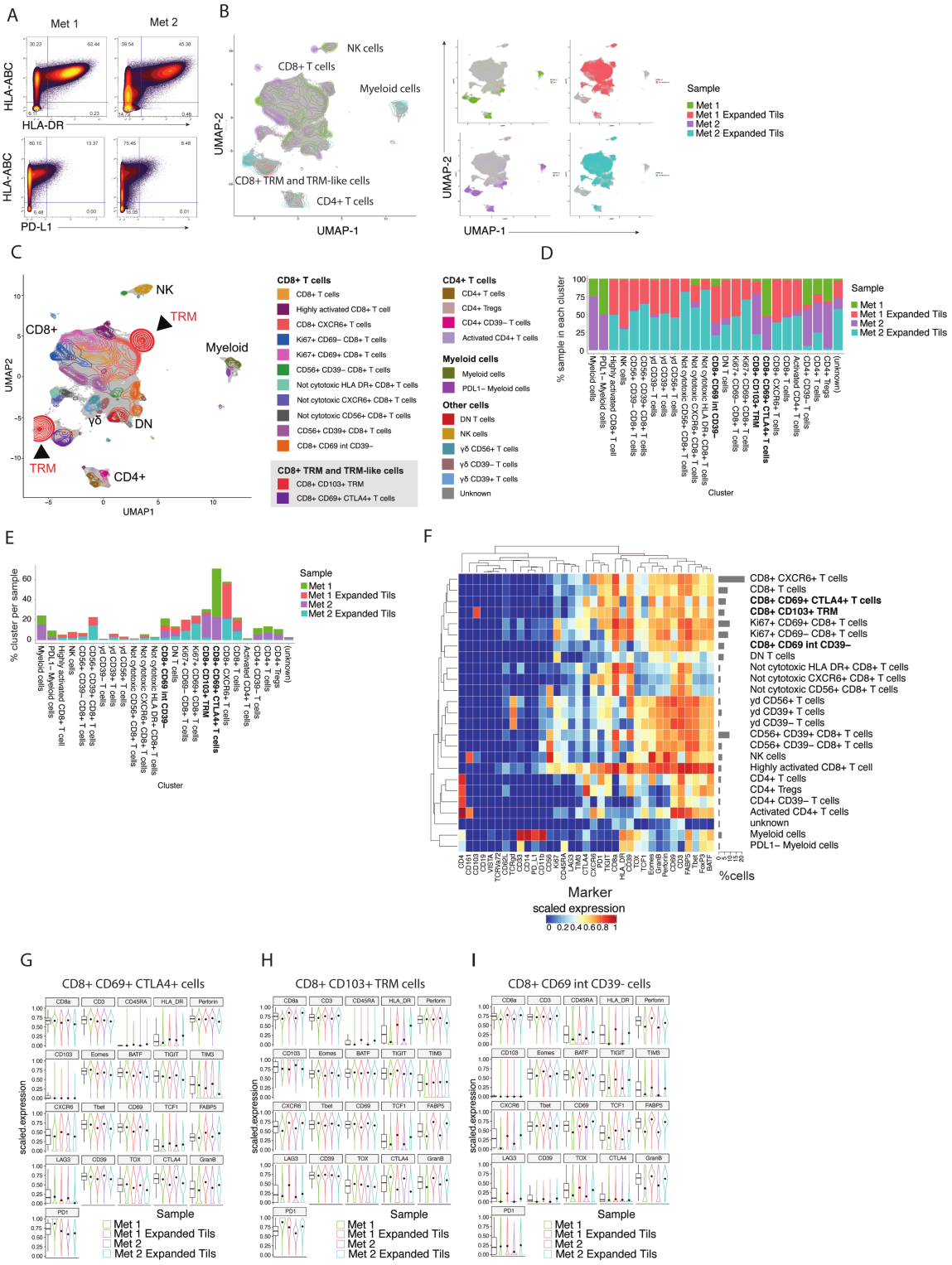

Figure 2 Mass cytometry revealed CD8$^+$ TRM cells were present across metastatic samples and expanded TILs. Mucosal melanoma TILs from Met1 and Met2 were either untreated, or expanded in vitro, and then analyzed by mass cytometry. Shown are (A) HLA-DR, HLA-ABC and PDL1 expression on CD45$^-$ live cells. Mass cytometry data from the four samples were collated into one file and analyzed by the FLOWSOM algorithm, TILs (CD45$^+$ HLA$^-$ABC$^+$ live cells) were clustered into 25 subsets based on protein expression in a UMAP display showing the distribution of individual samples (B) within the UMAP via contour (left) or colored clusters (right). Using the same UMAP display, also shown is the individual immune clusters as unique colored contours (C). Using the data from (B, C), the percentage of each sample was calculated for each cluster (D) and the percentage of each cluster represented in each sample (E). Also shown is the protein array data represented as a heat map for each immune cluster (F), and violin plots depicting scaled expression of select markers on CD8$^+$ TRM and related cell clusters (G–I) present in the tumor samples. TILs, tumor-infiltrating lymphocytes; TRM, tissue resident memory; UMAP, Uniform Manifold Approximation and Projection

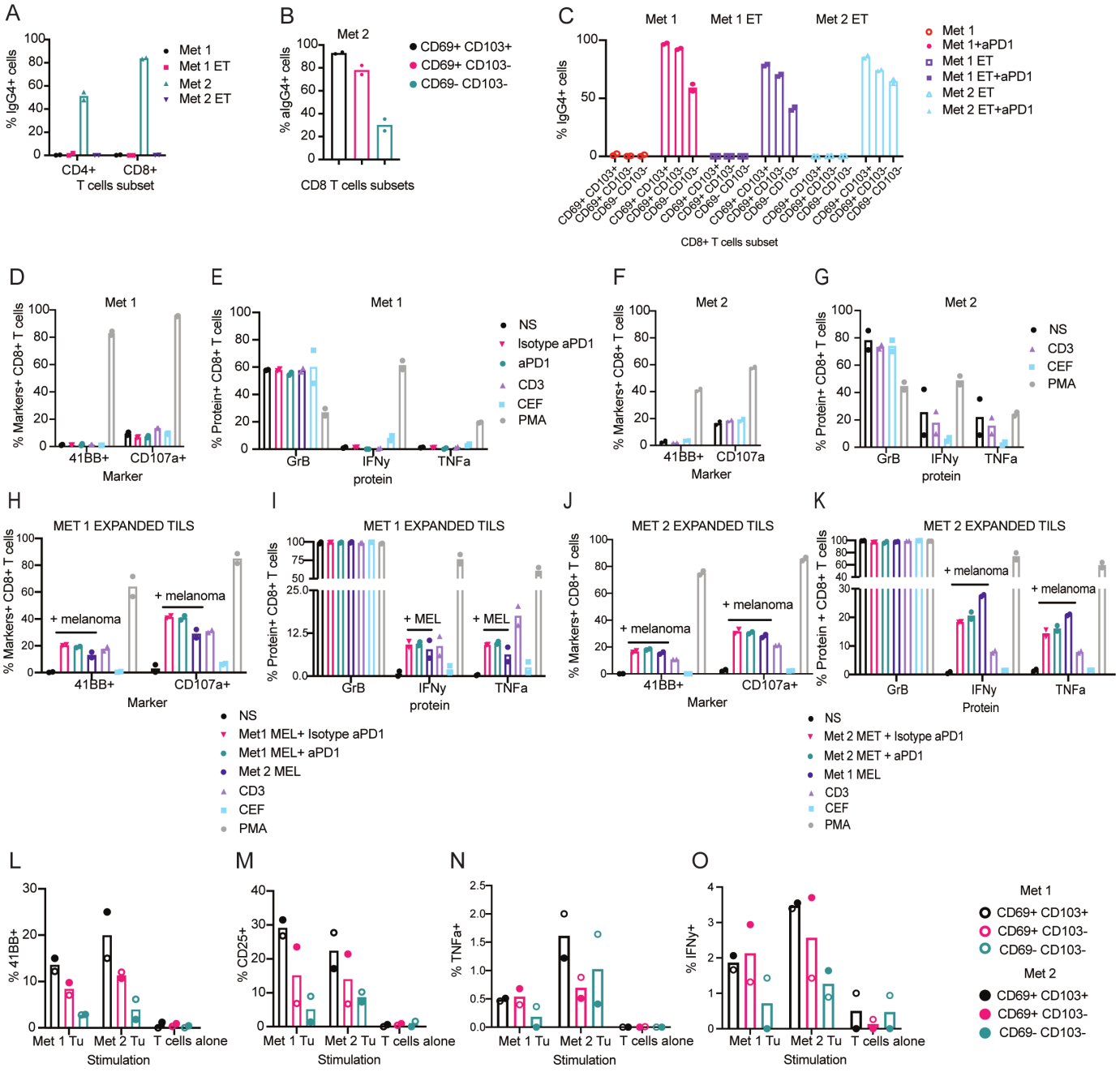

Figure 3 CD8⁺ TRM cells were the most tumor-responsive T cell cluster in mucosal melanoma. T cells isolated from the Met2 sample were bound with pembrolizumab. (A, B) In vivo administered pembrolizumab was detected on tumor samples by staining with anti-human IgG_4. (C) PD1 detection on Met1 TILs and expanded TILs via in vitro staining with pembrolizumab and detection with anti-human IgG4 (aPD1). ET=expanded TILs. (D–G) Tumor T cell responses to in vitro overnight stimulation of Met1 (D, E) or Met2 (F, G) samples after staining with pembrolizumab or isotype control or addition of different stimuli. (NS=non stimulated, CD3=CD3/CD28 Immunocult, PMA=PMA/Ionomycin, CEF=CEF Peptivator, aPD1=pembrolizumab). T cell responses were detected as (D, F) 41BB and CD107a expression (E, G) Granzyme B, IFN-γ or TNF expression. (H–K) In vitro overnight stimulation of expanded TILs from the Met1 or Met2 sample with FACS sorted melanoma cells at a 2:1 TILs: melanoma ratio from either the Met1 (Met1 MEL) or the Met2 (Met2 MEL). TILs were stained with pembrolizumab or Isotype control before adding them to melanoma cells. Other stimuli are added to the media in the absence of melanoma cells. (L–O) FACS sorted T cells subsets were cultured for 11 days in the presence of irradiated and IFN-γ-stimulated tumor lines derived from Met1 and Met2 (Met1 Tu and Met2 Tu) at 1:1 ratio, with cytokines IL7, IL25 and IL2. On day 11, T cells were re-stimulated with the same tumor cell line overnight in the presence of Golgi Plug (Brefeldin A) for cytokine production, or absence for 41BB upregulation. The experiment was conducted once and technical replicates are shown. TILs, tumor-infiltrating lymphocytes; TRM, tissue resident memory.

between Met1 and Met2 and were consistent with infiltration of resident T cells with high expression of immune checkpoint molecules. Of note, there was a higher abundance of $CD8^+$ TRM cells in Met2 (figure 2E and online supplemental figure S3B).

Tumor infiltrating $CD8^+$ TRM cells share clones between melanoma metastases

We investigated gene expression and TCR repertoire at a single cell level in FACS-sorted $CD45^+CD3^+$ T cells from the four samples: Met1, Met2, Met1 exp, and Met2 exp (figure 4A and online supplemental figure S4A). Supervised clustering of the samples and visualization using UMAP identified 14 distinct cell populations (figure 4B), classified using putative marker expression (online supplemental figure S4B–C): two $CD8^+CD103^+$ TRM clusters (TRM^{C2} and TRM^{C7}: *ITGAE*$^+$, *CD69*$^+$, *CD8A*$^+$), two $CD103^-$ TRM-like cell clusters (C0 and C1: *CD69*$^+$, *CD8A*$^+$, *ITGAE*$^-$, *RGS-1*$^+$), a TRM-precursor cluster [C3 (*IL7R*$^+$): TRM-p], a central memory T cell cluster (C11 (*TCF7*$^+$): T_{cm}), three effector T cell clusters (C4, C5, C8: T_{eff}), and other minor clusters including $CD4^+$ T cells (C9,10) and myeloid and dendritic cell populations (figure 4B and online supplemental figure S4C). Proliferating TRM^{C2} (eg, *MKI67*$^+$ and *BIRC5*$^+$) were consistently more numerous than activated TRM^{C7} (+ *TBX21*$^+$ and *XCL2*$^+$) in all samples, and were increased in Met2 + Met1 (online supplemental figures S3C and S4A). We combined these two TRM clusters for downstream analyses. $CD8^+$ TRM and TRM-like populations combined (clusters 0, 1, 2, 7) accounted for approximately half of all T cells (49.4%–51.27%) (figure 4C), and the relative proportion of TRM cells within all T cells was increased in Met2 compared with Met1 and similarly in expanded TILs (figure 4C). The majority of T cell clonotypes were present as single cells (singleton) (figure 4D), and doublets (2 cells) and expanded (three or more cells) clones combined represented similar proportions in all the samples (figure 4D). However, TRM cells in metastatic TILs (figure 4D**,** right) showed higher proportion of singletons compared with the general T cell population (figure 4D**,** left), indicating that TRM cells harbored less in vivo expanded clones compared with overall T cell population (figure 4D). Met1 and Met2 shared 21.0% and 18.5% of all T cell clones and TRM clones, respectively (figure 4E). Interestingly, comparing metastatic and expanded TILs, lower proportions of TCRs were shared among all T cells (8.44%–13.8%) than when considering only TRM clones in the metastases and all clones in the expanded TILs (17%–18.5%), suggesting a preferential expansion of TRM in the expanded TILs over the general T cell population (figure 4E). TRM clonotypes were also present in other T cell subsets following expansion (figure 4F). Met1 TRM clonotypes were distributed primarily in Met1 exp TRM-like cells while Met2 TRM clonotypes were similarly represented in Met2 exp TRM, TRM-like, TRM-p and T_{eff} subsets (figure 4F). Similarly, when determining the presence of TRM clonotypes among other T cell subsets within the same sample and corresponding expanded TILs, we observed that TRM clonotypes were shared with other TRM-like clusters, including *TCF7*$^+$ TRM-p and T_{eff} clusters (figure 4G). We identified that 18.6% (13 clones total) of Met1 TRM clones were shared with Met2 TRM clones (figure 4H). There was no preference for the proliferating or activating TRM types among those that were shared (online supplemental figure S5B). While a small number of TRM clones in Met1 and Met2 were identifiable in PBMC sample taken at the time of Met1 excision (online supplemental figure S5C), none of these shared TRM clones were identified in the circulation. Nearly all the shared TRM clones were present among other T cell clusters in all samples, with a preference for TRM-like and T_{eff} (figure 4H). Taken together, single-cell RNA sequencing revealed similar T cell subsets infiltrating both metastases, with an increase in $CD8^+$ TRM in Met2 compared with Met1. While most of the T cells had unique TCR sequences, clonotype sharing was observed between TRM cells in the two metastases, with TRM sharing their TCR preferentially with similar functional T cell subsets, including T_{eff} and TRM-like cells.

TRM bind preferentially in vivo administered pembrolizumab and respond to tumor cells on in vitro restimulation

The Met2 tumor was refractory to pembrolizumab treatment; this occurred despite pembrolizumab being present on the surface of both $CD8^+$ and $CD4^+$ T cells from the Met2 sample (figure 3A–C). Furthermore, $CD8^+CD69^+CD103^+$ TRM and $CD4^+CD69^+$ TRM cells expressed the highest levels of PD1 in both metastases (figure 3A–C and online supplemental figure S6A,B). Overnight incubation of the single-cell suspension of Met1 sample induced no activation nor cytokine production by $CD8^+$ T cells (figure 3D–E) nor $CD4^+$ T cells (online supplemental figure S6C,D). In contrast, $CD8^+$ T cells expressed higher levels of CD107a and produced more intracellular granzyme B, interferon-γ (IFNγ) and tumor necrosis factor-α (TNFα) after overnight incubation of the single-cell suspension of Met2 (figure 3F–G) compared with Met1, and a similar effect was visible in $CD4^+$ T cells (online supplemental figure S6E,F). $CD8^+$ T cells in expanded TILs from both metastatic samples upregulated 41BB and CD107a expression and produced IFNγ and TNFα on contact with autologous tumor cells (figure 3H–K), whereas $CD4^+$ T cells responded to a much lower extent to autologous tumor (online supplemental figure S6G,J). Interestingly, expanded TIL $CD8^+$ and $CD4^+$ T cells also responded to tumor cells from the other autologous metastasis, suggesting that the antigen(s) recognized were conserved or public (figure 3H–K, online supplemental figure S6G,J). Viral peptides (CEF) did not activate T cells in neither the freshly isolated TILs nor expanded TILs, indicating that viral-specific bystander T cells reactive were not present in the tumors (figure 3H–K). $CD8^+$ T cells were FACS-sorted into $CD69^+CD103^+$ TRM, $CD69^+$ and $CD69^-$ subsets and then cultured with tumor cells overnight. Only T cells derived from the expanded TILs,

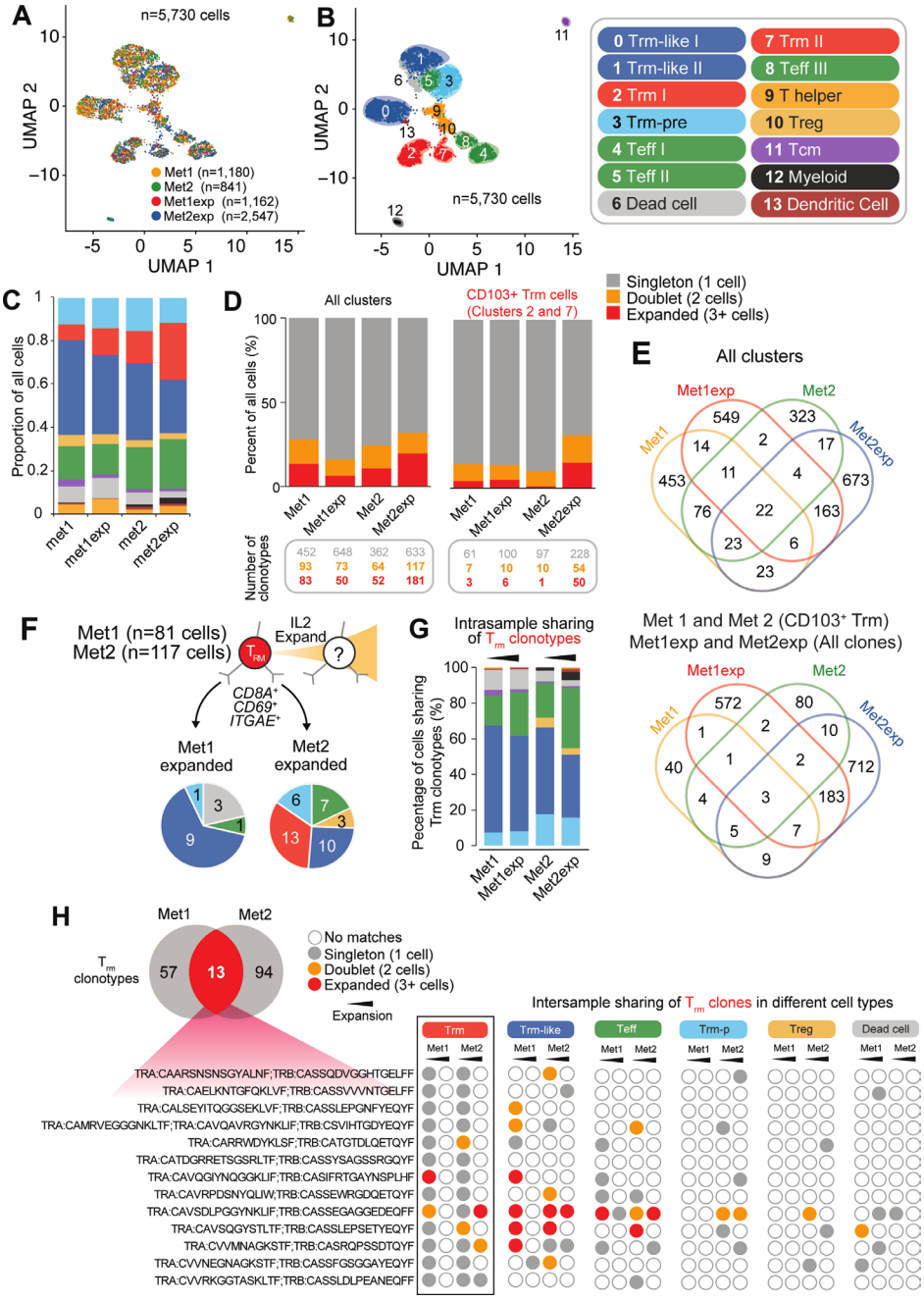

Figure 4 Single-cell gene expression and TCR sequencing revealed dynamic tissue-resident T cell populations at multiple metastatic sites. (A) UMAP dimensionality reduction of tumor tissue T cell populations (Met1 and Met2) and corresponding expanded T cell samples (Met1exp and Met2 exp). Following sequencing and T-cell specific filtering we obtained a total of 5730 cells across four samples (Met1: 1180, Met2: 841, Met1 exp: 1162 and Met2 exp: 2,547). (B) Principal component analysis and cluster identification of 13 cell populations among all 5730 cells in analysis. Cell phenotypes determined using cluster markers within cell markers to include TRM-like (blue: $CD8A^+$, $CD69^+$, $CD103^-$), TRM (red: $CD8A^+$, $CD69^+$, $CD103^+$), T_{cm} central memory T cells (purple), effector T_{eff} cells (green), CD4 helper and Tregs (yellow), myeloid cells (black), dendritic cells (brown) and dead cells (gray). (C) Distribution of cell phenotype proportions in four samples following the amalgamation of similar cell types from B. (D) Paired αβ T cell receptor expansion analysis of all cells (left panel) and TRM cells only (right panel) from four samples and corresponding proportions of singleton clones (1 cell), doublets (2 cells with matching clonotype), and expanded clones (≥3 cells per matching clonotype). The total number of clonotypes in each category is shown in the table below. (E) Venn diagram depicting individual clonotype sharing between all four samples for all clusters (upper) and TRM cells only (lower). (F) Pie charts indicating conversion of TRM to other T cell phenotypes in Met1 (81 cells) and Met2 (117 cells) tissue samples following high dose IL^-2 expansion (Met1 exp and Met2 exp). Matching αβ T cell receptor sequences were used to track cell phenotypes between samples. (G) Identification of the proportion of cells in non^-TRM clusters also harboring a TRM $αβ^-TCR$. High-dose IL2 expansion of tissue TILs indicated. (H) Shared TRM clonotypes (n=13) between Met1 and Met2 samples showing distribution in other T cell phenotypes and samples in the analysis according to the singlet, doublet and expanded status. TCR, T cell receptor; TRM, tissue resident memory.

but not from tumor samples, upregulated CD107a after overnight contact with the autologous tumor cells (online supplemental figure S6K–N). To determine the capacity of CD8$^+$ T cell subsets to harbor tumor-responsive progeny, we cultured FACS-sorted CD8$^+$CD69$^+$ CD103$^+$ TRM, CD69$^+$ and CD69$^-$ T subsets, derived from Met1 and Met2, with irradiated autologous tumor cell lines for 10 days and then re-challenged them with the same cell lines overnight and measured response by upregulation of CD25 or 41BB. Progeny of TRM cells was more activated in contact with the tumor, irrespective of metastasis of origin or tumor line used for stimulation, compared with CD69$^+$ and CD69$^-$ T cell subsets (figure 3L–O). Taken together, these data strongly suggest that VM CD8$^+$ TRM cells from this patient harbor a higher proportion of tumor-responsive T cells compared with other T cell subsets, and that prolonged antigen stimulation in the presence of T cell-stimulating cytokines can reinvigorate their capacity to respond to the tumor.

Expanded TILs recognize a conserved neoantigen

Whole exome sequencing of tumor samples defined single nucleotide variants, insertion/deletions and copy number variations specific of the melanoma site, which are very similar between the two metastatic lesions and typical of mucosal melanoma with low mutational load (figure 5A,B).[20] Most of these mutations were shared between the two metastatic tumors, confirming their common lineage (figure 5A,B). These mutations are characteristic of several mutational processes, including age, tobacco exposure and defective DNA repair (figure 5C). Neoantigens were identified by selecting DNA mutated proteins that were expressed at the RNA level and predicted to bind MHC-I or MHC-II alleles of the patient. Of the 38 predicted neoantigens, 31 occurred in regions predicted to bind both MHC I and MHC II and 24 were common to both lesions. Of note, Met2 expressed the majority of the private neoantigens (12 vs 2 in Met1), suggesting ongoing evolution (figure 5D). Six of the 38 neoantigens were shared between the Mets and the primary sample, supporting the clonal origin of the metastases (figure 5D). We first tested the response of expanded TILs to predicted neoantigens selecting all the peptides of each protein for which at least one neoantigen was predicted to be a strong binder to MHC-I and -II (online supplemental tables 4,5). To examine T cell responses to these antigens autologous LCL cells were pulsed with predicted neoantigen peptide pools and co-cultured with Met1 and Met2 expanded TILs for 10 days, before a short rechallenge with the same stimuli. CD8$^+$ T cells in Met1 and Met2 expanded TILs responded to a neoantigen peptide pool of protein CDKN1C (LCL-017) and not to the corresponding wild type peptides (LCL-wt peptides), as well as a pool of melanoma differentiation antigens of Gp100 and Tyrp2 (Known_2, online supplemental table 6) by producing IFNγ and TNFα and upregulating CD107a (figure 5E and online supplemental figure S6O). CD8$^+$ T cells in Met1 and Met2 expanded TILs also responded to autologous melanoma cells at a higher level than that observed with LCL-017 or melanoma differentiation antigens, suggesting these TILs have other tumor antigen specificities (figure 5E and online supplemental figure S6O). In summary, we identified a mutation in the negative regulator of cell cycle (CDKN1C) expressed in the primary tumor and shared by both metastases, which is recognized by in vitro expanded CD8$^+$ T cells generated from both metastases.

DISCUSSION

Here, we described the immunological profile of a patient with VM, a melanoma subtype with low response to ICB. We used three longitudinal samples of primary and metastatic disease from a patient refractory to all conventional therapies, including ICB. Using this unique sample set, we defined CD8$^+$ T cell function, gene expression and clonality. We found that tumor-infiltrating CD8$^+$ T and TRM cells were tumor-responsive after prolonged in vitro co-culture in the presence of cytokines, but not after brief contact with tumor cells, indicating profound immune-suppression in vivo (figure 3). These findings correlate to those reported in metastatic cutaneous melanoma and head and neck squamous cell carcinoma.[26 27] Unique to our study is the finding that we can rescue the capacity of TRM to respond to the tumor in a culture with IFNγ-stimulated tumor cells, suggesting that this effect could occur in a T cell infiltrated tumor in vivo. We also showed a spectrum of coexisting 'exhausted' T cell populations in the tumor. These were characterized by distinct levels of proliferation, cytotoxicity and response to anti-PD1 stimulation,[27–29] suggesting that some populations of tumor infiltrating T cells are not exhausted and can indeed be tumor-responsive, as indicated in lung cancer.[30 31] The most recent research, including our study, revealed that TRM cells are in close proximity to tumor cells (figure 1)[32] and their activation results in tumor recognition (figure 5)[26] that can trigger other arms of immunity, including dendritic cells and B cells, favoring epitope spreading.[33–35] TRM and T cells proliferate and infiltrate metastatic melanoma after anti-PD1 treatment[11 36] and concordantly even in this mucosal melanoma patient, TRM increased longitudinally after administration of anti-PD-1 (figures 2 and 4). In several cancer types, ICB treatment induces a shift in T cell clonality, suggesting in vivo epitope-spreading and de novo T cell priming and recruitment, and selective clonal expansion is associated with clinical benefit.[37–40] Similarly, in our study, only approximately 10% of all clonotypes were shared between the metastatic sites. However, interestingly, a larger proportion of TRM clonotypes (18%) were shared, suggesting an effect of the tumor antigens or chemokine/cytokine signaling in recruiting pre-TRM consistently to tumor sites.

Indeed, the metastatic tumors shared most mutations and neoantigens, and the only neoantigen that was recognized by expanded TILs was conserved between the two

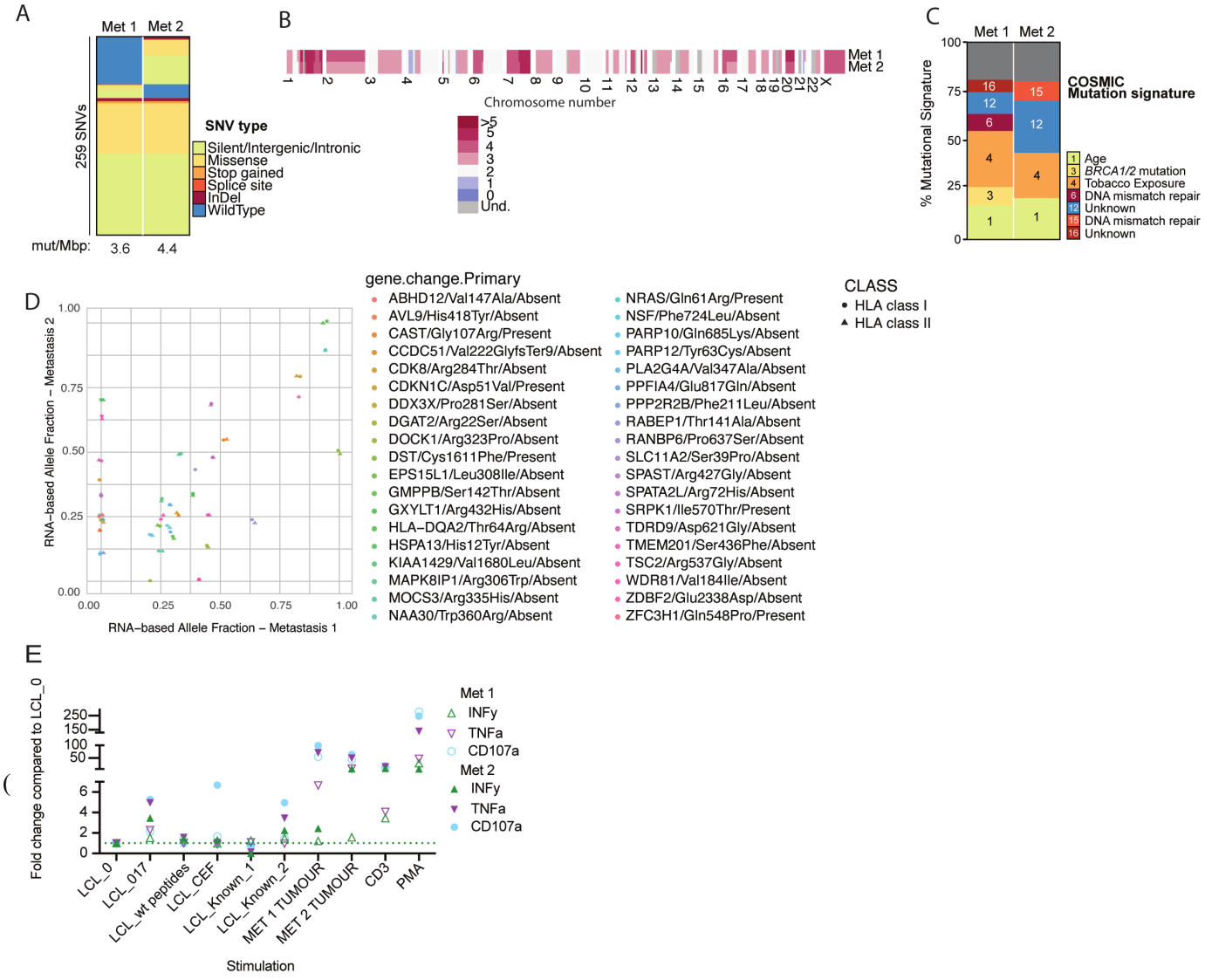

Figure 5 Metastases shared neoantigens and similar mutational profiles corresponding to a mucosal clonal origin of tumor cells. (A) Tumor genomic mutations. Each row represents a mutation (259 in total), and each column represents a sample. 'Wild-type' indicates absent mutations in a given sample. Color indicates the type of mutation. (B) Copy number variations are represented per chromosome and a color scale to indicate the number of detected alterations per region. (C) Mutational signatures as identified using version 2 of the COSMIC database. (D) Predicted neoantigens for MHC class I and MHC class II. The allele fraction of expressed mutations observed in the RNA-Seq data is shown for Met1 (x-axis) vs Met2 (y-axis). The expression status of each mutation in the primary sample is indicated as absent/present in the legend. (E) Fold ratio of cytokine production and CD107a expression within $CD8^+$ T cells after 3.5 hours in vitro restimulation of expanded TILs with irradiated autologous lymphoblastoma cell line (LCL) coated with neoantigen peptides or with IFN-γ-stimulated autologous melanoma cell lines. The cytokine production ratio is calculated compared with non-peptide pulsed LCL (LCL-0). As controls, cells were restimulated with Immunocult (a-CD3/a-CD28) or PMA. Expanded TILs were previously cultured for 11 days in the presence of the same stimuli used for the restimulation. The experiment was conducted once. MHC, major histocompatibility complex; TILs, tumor-infiltrating lymphocytes.

sites. It remains to be revealed whether these neoantigen-specific T cells were generated from TRM clones, an arduous task given the low frequency of neoantigen-specific T cells among expanded TILs, the dramatic loss of clonotype diversity in expanded TILs (figure 4)[41], and the modest levels of T-cell expansion within the tissue, with ~25% of clonotypes being expanded (2 cells or more), as reported also in cutaneous melanoma.[27] The expansion of T cells could have been underestimated due to low number of cells analyzed. Moreover, since the intercluster and intracluster sharing of clonotypes was common, including between TRM and other related cell phenotypes, tracking the clonotypes of the antigen-specific T cells would only indicate which spectrum of differentiation they were derived from. The TRM were very similar in two distant VM metastases. Furthermore, their gene expression, phenotype and functionality are akin to T cells in cutaneous melanoma and other cancer types, pointing toward tumor or other cell type-intrinsic factors to explain the resistance of this tumor type to

ICB, such as low mutation rate, low neoantigen load and, therefore, very limited priming of antitumor T cells. In addition, we observed partial loss of VM MHC-I expression in the second metastasis, this loss of antigen expression could be pivotal in loss of T cell and, in particular, TRM activity. A direct comparison with a larger number of samples would be necessary to confirm these findings.

While it is encouraging that TRM antitumor function persist in distinct distant VM metastases of this patient, it is clear that anti-PD1 or anti-CTLA4 monotherapy was not sufficient to rescue the TRM activity in vivo in this signature VM case. RT is known to modify the tumor microenvironment leading to priming of T cells to tumor-derived antigen and, when used in combination with anti-CTLA4, abscopal responses in a patients with metastatic cutaneous melanoma.[4243] Indeed, a recent study showed a patient with metastatic VM responded to the combination of RT and ICB[44] using a combination of hypofractionated and low dose RT to distinct metastases. In our VM case, the patient received nivolumab plus RT to multiple metastatic sites, including the tissue analyzed as Met 2, but this disease remained resistant to combination RT and ICB.

In summary, our study revealed that primary VM is an immunologically cold tumor in our patient as well as in a bigger cohort. We showed that tumor-responsive TRMs were present at the tumor margin in both VM metastases from the same patient. The TRM cluster responded at the highest level to both neoantigens and melanoma differentiation antigens and, therefore, remain a potent component of the antitumor immune response, which may have been rendered ineffective in vivo due to partial loss of VM MHC-I expression.

Author affiliations
[1]Sir Peter MacCallum Department of Oncology, The University of Melbourne, Melbourne, Victoria, Australia
[2]Cancer Immunology Program, Peter MacCallum Cancer Centre, Melbourne, Victoria, Australia
[3]Peter MacCallum Cancer Centre, Melbourne, Victoria, Australia
[4]Tumor Suppression Laboratory, Peter MacCallum Cancer Centre, Melbourne, Victoria, Australia
[5]Melanoma Institute Australia, Camperdown, New South Wales, Australia
[6]Faculty of Medicine and Health, The University of Sydney, Sydney, NSW, Australia
[7]Australian Genome Research Facility Ltd, Melbourne, Victoria, Australia
[8]Division of Cancer Research, Peter MacCallum Cancer Centre, Melbourne, Victoria, Australia
[9]Medical Oncology, Peter MacCallum Cancer Centre, Melbourne, Victoria, Australia
[10]Division of Cancer Surgery, Peter MacCallum Cancer Centre, Melbourne, Victoria, Australia
[11]F Hoffmann-La Roche Ltd, Basel, Switzerland

Twitter Jafar Jabbari @jafarjabbari and David E Gyorki @davidgyorki

Acknowledgements The authors would like to acknowledge the staff at the flow cytometry facility and the Centre for Advanced Histology and Microscopy (CAHM) at PeterMac for their valuable help, as well as Pasquale Petrone, Thu Nguyen and Han Aw Yeang for technical assistance.

Contributors PJN conceived the project and MP oversaw the project. AP, SPK and PJN designed the experiments, AP, SPK, NK, DT, JJ performed the experiments. AP, SPK, IAV, FC, ATP, NK, NT, MW analyzed the data. GA-Y, SS, DEG and AW provided the samples and the clinical history of the patient. AP, SPK and PJN wrote the manuscript. All coauthor provided intellectual input in the project and revised the manuscript. PN is the guarantor for this manuscript.

Funding This project was funded by an imCORE project funds, F. Hoffmann-La Roche, to PJN.

Competing interests AP, NK and SPK were supported by imCORE, F. Hoffmann-La Roche. MP is an employee of F. Hoffmann-La Roche. DEG has been on advisory board for Amgen, Q Biotics, Provectus and Bayer. SS has been receiving advisory board fees, paid to her institution, and grant support from AstraZeneca and Merck Sharp & Dohme, and grant support from Amgen, Endocyte, and Genentech.

Patient consent for publication Consent obtained directly from patient(s)

Ethics approval This study involves human participants and was approved by Ethics ID 13/141.Peter MacCallum Cancer Centre ethics committee.

Provenance and peer review Not commissioned; externally peer reviewed.

Data availability statement Data are available on reasonable request. We are in the process to upload the data in dbGAP. It will be available on request as per our institute policy.

ORCID iDs
Angela Pizzolla http://orcid.org/0000-0003-2024-4144
Simon Paul Keam http://orcid.org/0000-0001-9053-9138
Minyu Wang http://orcid.org/0000-0002-1051-5855
Paul Joseph Neeson http://orcid.org/0000-0002-2729-5887

REFERENCES

1 Nobbenhuis MAE, Lalondrelle S, Larkin J, *et al*. Management of melanomas of the gynaecological tract. *Curr Opin Oncol* 2014;26:508–13.
2 Mihajlovic M, Vlajkovic S, Jovanovic P, *et al*. Primary mucosal melanomas: a comprehensive review. *Int J Clin Exp Pathol* 2012;5:739–53.
3 Sanchez A, Rodríguez D, Allard CB, *et al*. Primary genitourinary melanoma: epidemiology and disease-specific survival in a large population-based cohort. *Urol Oncol* 2016;34:166.e7–166.e14.
4 St Clair C, Wethington S, Eaton A, eds. *Vulvar and vaginal melanoma——a single institutional experience 1995–2012*. 44th Annual Meeting on Women's Cancer, 2013.
5 Hou JY, Baptiste C, Hombalegowda RB, *et al*. Vulvar and vaginal melanoma: a unique subclass of mucosal melanoma based on a comprehensive molecular analysis of 51 cases compared with 2253 cases of nongynecologic melanoma. *Cancer* 2017;123:1333–44.
6 Newell F, Kong Y, Wilmott JS, *et al*. Whole-genome landscape of mucosal melanoma reveals diverse drivers and therapeutic targets. *Nat Commun* 2019;10:3163.
7 D'Angelo SP, Larkin J, Sosman JA, *et al*. Efficacy and safety of nivolumab alone or in combination with ipilimumab in patients with mucosal melanoma: a pooled analysis. *J Clin Oncol* 2017;35:226–35.
8 Furney SJ, Turajlic S, Stamp G, *et al*. Genome sequencing of mucosal melanomas reveals that they are driven by distinct mechanisms from cutaneous melanoma. *J Pathol* 2013;230:261–9.
9 Taylor RC, Patel A, Panageas KS, *et al*. Tumor-Infiltrating lymphocytes predict sentinel lymph node positivity in patients with cutaneous melanoma. *J Clin Oncol* 2007;25:869–75.
10 Song H, Wu Y, Ren G, *et al*. Prognostic factors of oral mucosal melanoma: histopathological analysis in a retrospective cohort of 82 cases. *Histopathology* 2015;67:548–56.
11 Edwards J, Wilmott JS, Madore J, *et al*. CD103$^+$ Tumor-Resident CD8$^+$ T Cells Are Associated with Improved Survival in Immunotherapy-Naïve Melanoma Patients and Expand Significantly During Anti-PD-1 Treatment. *Clin Cancer Res* 2018;24:3036–45.

12 Savas P, Virassamy B, Ye C, *et al*. Single-cell profiling of breast cancer T cells reveals a tissue-resident memory subset associated with improved prognosis. *Nat Med* 2018;24:986–93.
13 Malik BT, Byrne KT, Vella JL, *et al*. Resident memory T cells in the skin mediate durable immunity to melanoma. *Sci Immunol* 2017;2. doi:10.1126/sciimmunol.aam6346. [Epub ahead of print: 14 Apr 2017].
14 Park CO, Fu X, Jiang X, *et al*. Staged development of long-lived T-cell receptor αβ T_H17 resident memory T-cell population to Candida albicans after skin infection. *J Allergy Clin Immunol* 2018;142:647–62.
15 Rosenberg SA, Yannelli JR, Yang JC, *et al*. Treatment of patients with metastatic melanoma with autologous tumor-infiltrating lymphocytes and interleukin 2. *JNCI Journal of the National Cancer Institute* 1994;86:1159–66.
16 Halse H, Colebatch AJ, Petrone P, *et al*. Multiplex immunohistochemistry accurately defines the immune context of metastatic melanoma. *Sci Rep* 2018;8:11158.
17 Van Gassen S, Callebaut B, Van Helden MJ, *et al*. FlowSOM: using self-organizing maps for visualization and interpretation of cytometry data. *Cytometry A* 2015;87:636–45.
18 Crowell HZV, Chevrier S. *Robinson M catalyst: cytometry dATa anALYSis tools*. R package version 1.18.0, 2021.
19 Wilkerson MD, Hayes DN. ConsensusClusterPlus: a class discovery tool with confidence assessments and item tracking. *Bioinformatics* 2010;26:1572–3.
20 Melville J. uwot: the uniform manifold approximation and projection (UMAP) method for dimensionality reduction.
21 Gu Z, Eils R, Schlesner M. Complex heatmaps reveal patterns and correlations in multidimensional genomic data. *Bioinformatics* 2016;32:2847–9.
22 Wickham H. *ggplot2: elegant graphics for data analysis*. New York: Springer-Verlag, 2016.
23 Stuart T, Butler A, Hoffman P, *et al*. Comprehensive integration of single-cell data. *Cell* 2019;177:1888–902.
24 Budhwani M, Mazzieri R, Dolcetti R. Plasticity of type I interferon-mediated responses in cancer therapy: from anti-tumor immunity to resistance. *Front Oncol* 2018;8:322.
25 Mikkelsen LH, Maag E, Andersen MK, *et al*. The molecular profile of mucosal melanoma. *Melanoma Res* 2020;30:533–42.
26 Duhen T, Duhen R, Montler R, *et al*. Co-expression of CD39 and CD103 identifies tumor-reactive CD8 T cells in human solid tumors. *Nat Commun* 2018;9:2724.
27 Li H, van der Leun AM, Yofe I, *et al*. Dysfunctional CD8 T cells form a proliferative, dynamically regulated compartment within human melanoma. *Cell* 2019;176:775–89.
28 Gueguen P, Metoikidou C, Dupic T, *et al*. Contribution of resident and circulating precursors to tumor-infiltrating $CD8^+$ T cell populations in lung cancer. *Sci Immunol* 2021;6. doi:10.1126/sciimmunol.abd5778. [Epub ahead of print: 29 01 2021].
29 Miller BC, Sen DR, Al Abosy R, *et al*. Subsets of exhausted $CD8^+$ T cells differentially mediate tumor control and respond to checkpoint blockade. *Nat Immunol* 2019;20:326–36.
30 Corgnac S, Malenica I, Mezquita L, *et al*. $CD103^+CD8^+T_{RM}$ Cells Accumulate in Tumors of Anti-PD-1-Responder Lung Cancer Patients and Are Tumor-Reactive Lymphocytes Enriched with Tc17. *Cell Rep Med* 2020;1:100127.
31 Clarke J, Panwar B, Madrigal A, *et al*. Single-cell transcriptomic analysis of tissue-resident memory T cells in human lung cancer. *J Exp Med* 2019;216:2128–49.
32 Egelston CA, Avalos C, Tu TY, *et al*. Human breast tumor-infiltrating $CD8^+$ T cells retain polyfunctionality despite PD-1 expression. *Nat Commun* 2018;9:4297.
33 Boddupalli CS, Bar N, Kadaveru K, *et al*. Interlesional diversity of T cell receptors in melanoma with immune checkpoints enriched in tissue-resident memory T cells. *JCI Insight* 2016;1:e88955.
34 Menares E, Gálvez-Cancino F, Cáceres-Morgado P, *et al*. Tissue-resident memory $CD8^+$ T cells amplify anti-tumor immunity by triggering antigen spreading through dendritic cells. *Nat Commun* 2019;10:4401.
35 Workel HH, Lubbers JM, Arnold R, *et al*. A Transcriptionally Distinct $CXCL13^+CD103^+CD8^+$ T-cell Population Is Associated with B-cell Recruitment and Neoantigen Load in Human Cancer. *Cancer Immunol Res* 2019;7:784–96.
36 Sade-Feldman M, Jiao YJ, Chen JH, *et al*. Resistance to checkpoint blockade therapy through inactivation of antigen presentation. *Nat Commun* 2017;8:1136.
37 Riaz N, Havel JJ, Makarov V, *et al*. Tumor and microenvironment evolution during immunotherapy with nivolumab. *Cell* 2017;171:934–49.
38 Wu TD, Madireddi S, de Almeida PE, *et al*. Peripheral T cell expansion predicts tumour infiltration and clinical response. *Nature* 2020;579:274–8.
39 Yost KE, Satpathy AT, Wells DK, *et al*. Clonal replacement of tumor-specific T cells following PD-1 blockade. *Nat Med* 2019;25:1251–9.
40 Corgnac S, Botelho NK, Donda A, *et al*. Recombinant fusion proteins for targeting dendritic cell subsets in therapeutic cancer vaccine. *Methods Enzymol* 2020;632:521–43.
41 thor Straten P, Kirkin AF, Siim E, *et al*. Tumor infiltrating lymphocytes in melanoma comprise high numbers of T-cell clonotypes that are lost during in vitro culture. *Clin Immunol* 2000;96:94–9.
42 Twyman-Saint Victor C, Rech AJ, Maity A, *et al*. Radiation and dual checkpoint blockade activate non-redundant immune mechanisms in cancer. *Nature* 2015;520:373–7.
43 Postow MA, Callahan MK, Barker CA, *et al*. Immunologic correlates of the abscopal effect in a patient with melanoma. *N Engl J Med* 2012;366:925–31.
44 Sezen D, Patel RR, Tang C, *et al*. Immunotherapy combined with high- and low-dose radiation to all sites leads to complete clearance of disease in a patient with metastatic vaginal melanoma. *Gynecol Oncol* 2021;161:645–52.